Journal of Biomedical Optics 8(4), 648–654 (October 2003)

Hand-held arthroscopic optical coherence tomography for *in vivo* high-resolution imaging of articular cartilage

Yingtian Pan*
State University of New York, Stony Brook
Department of Biomedical Engineering
Stony Brook, New York 11794-8181
and
University of Pittsburgh
Department of Medicine
3550 Terrace Street
Pittsburgh, Pennsylvania 15261
E-mail: yingtian.pan@sunysb.edu

Zhigang Li
Tuqiang Xie
University of Pittsburgh
Department of Medicine
3550 Terrace Street
Pittsburgh, Pennsylvania 15261

Constance R. Chu
University of Pittsburgh
Department of Orthopedic Surgery
3550 Terrace Street
Pittsburgh, Pennsylvania 15261
E-mail: chucr@msx.upmc.edu

Abstract. We describe a novel hand-held polarization optical coherence tomographic (OCT) probe that can be inserted into mammalian joints to permit real-time cross-sectional imaging of articular cartilage. The transverse and axial resolutions of the arthroscopic OCT device are roughly 17 and 10 μm, respectively. Two-dimensional cross-sectional images of cartilage tissue with 500×1000 pixels covering an area 6 mm in length and 2.8 mm in depth can be acquired at nearly five frames/s and with over 100 dB of dynamic range. Design of an OCT as a hand-held device capable of providing such an optical biopsy of articular cartilage allows eventual *in vivo* detection of microstructural changes in articular cartilage that are not apparent using conventional arthroscopic cameras. The OCT probe can be easily incorporated in a conventional arthroscope for cartilage site guidance. The optical arrangement in the OCT scope minimizes specular back-reflection of the probe end face and absorption of body fluid in the path and ensures in-focus OCT imaging when it is in contact with the cartilage specimen to be examined. Successful application of *in vivo* arthroscopy to porcine articular cartilage demonstrates sufficient resolution and practicality for use in human joints. [DOI: 10.1117/1.1609201]

Keywords: optical coherence tomography; arthroscopy; laser scanning arthroscopy; articular cartilage; polarization contrast imaging; osteoarthritis.

Paper 02083 received Dec. 2, 2002; revised manuscript received May 30, 2003; accepted for publication Jun. 19, 2003.

1 Introduction

The demand for noninvasive or minimally invasive and high-resolution clinical diagnosis has led to several emerging optical imaging techniques,[1–3] among which optical coherence tomography (OCT) has attracted the attention of researchers and clinicians in the field.[4] OCT uses the low-coherence property of broadband light and backscattering signatures of cells to image tissue morphology at a high resolution (e.g., 2 to 10 μm). Since its early introduction to image the interior of the eye,[5] OCT has demonstrated important implications for high-resolution diagnosis of a variety of ocular diseases.[6] Despite the challenges of multiple scattering, this technique has been extensively studied in imaging a wide variety of nontransparent tissues with high resolution and dynamic range (>100 dB), which includes skin, teeth, vascular tissue, and gastrointestinal, respiratory, and genitourinary tracts, as well as malformations in these tissues.[7–11] Recent technological advances have permitted ultrahigh resolution (2 to 5 μm) OCT, polarization-sensitive OCT (PSOCT), Doppler OCT, and spectroscopic OCT to enhance image contrast and resolution.[12–15] More important, as a fiber optically based imaging technology, OCT can be integrated with conventional endoscopic techniques. Several endoscopic OCT imaging probes have been reported by implementing different optical delivery-scan-collection mechanisms, including catheter-endoscopic OCT probes using a rotary 90-deg prism,[9] a piezoelectric transducer (PZT) swing scanner,[16] and a microelectromechanical (MEMS) mirror.[17] Like conventional endoscopy that has developed into different specialties (e.g., cystoscopy, arthroscopy, and laparoscopy) to satisfy different requirements, different OCT endoscopies need to be developed to tackle different accessibility and light scanning requirements as well as to provide specific image contrast enhancement in different tissues.

Articular cartilage injury is a common clinical disease that involves degeneration of subsurface lesions.[18] Noninvasive early detection of these lesions and staging their progression would result in important therapeutic benefits to patients. Because of superior resolution and intermediate image depth (e.g., 1 to 3 mm), several research groups have reported the use of OCT to image articular cartilage architectures and defects in these tissues, showing great promise for potential clinical diagnosis.[19–21] In particular, PSOCT has shown interesting birefringence contrast related to collagen orientations in the cartilage,[22] which in turn promotes the development of more advanced PSOCT techniques.[23,24]

*Address questions regarding arthroscopic OCT probe design and imaging to Dr. Pan, and those regarding medical implications to Dr. Chu.

1083-3668/2003/$15.00 © 2003 SPIE

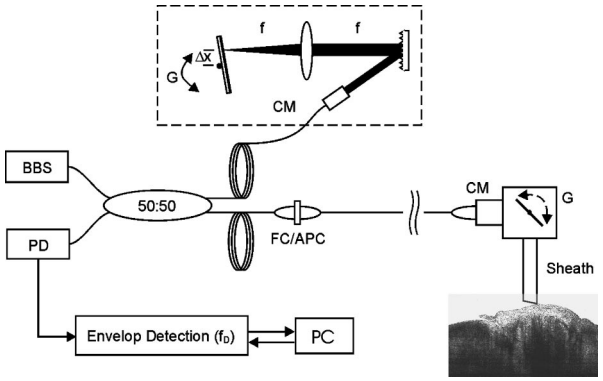

Fig. 1 Schematic of a real-time OCT arthroscope. A detailed sketch of the hand-held OCT probe is given in Fig. 2. BBS, broadband source; PD, photodiode; CM, fiber optic collimator; G, servomirror.

Our recent results based on *ex vivo* studies demonstrated that OCT could detect microstructural changes in articular cartilage associated with cartilage injury, degeneration, and repair (e.g., fibrillation, embedded tears, indentation, and degeneration) in animal repair models.[25] These results support the development of an OCT probe designed for real-time, *in vivo* imaging of articular cartilage. We report the development of a near-real-time polarization arthroscopic OCT device. Although PSOCT has been extensively studied,[26] we use a simple rotary polarizer to separate cartilage structural defects and birefringence patterns. The design of the hand-held OCT probe, along with the results of arthroscopic examination of articular cartilage in porcine knee joints is reported. These preliminary results suggest that arthroscopic OCT can be used for minimally invasive diagnosis of cartilage injuries and immediate assessment of treatment results.

2 Arthroscopic OCT Probe

The new arthroscopic OCT device was developed by connecting the sample arm of a fiber optic OCT setup with a hand-held arthroscopic probe. Optical coherence tomography uses optical coherence-domain reflectometry to detect the path length-resolved reflections of light from within the scattering media.[5] Unlike conventional microscopy, axial sectioning in most OCT imaging (except optical coherence microscopy) is accomplished by scanning the reference mirror; thus it circumvents the need to axially scan the objective lens in the sample arm, which is critical to the implementation of laser scanning endoscopy. The principle of OCT and the technical details of our real-time OCT setup have been previously reported;[25] therefore, only a brief introduction is given here. Figure 1 is a schematic diagram of the overall arthroscopic OCT setup.

A broadband laser source (BBS) was coupled into the input monomode fiber to illuminate the fiber optic Michelson interferometer. The center wavelength and the spectral bandwidth of the BBS source were $\lambda_0 = 1310$ nm and $\Delta\lambda = 77$ nm, respectively, yielding a source coherence length of $L_c = 10\ \mu$m.[25] The pigtailed output power P of the light source was 12 mW. The light from the BBS source was split equally into the reference and sample arms of the fiber optic Michelson interferometer. In the reference arm, the light exiting the fiber end face was collimated to a ϕ2-mm Gaussian beam by a fiber optic asperical lens (CM), and delivered to a high-speed depth-scanning unit, e.g., a rapid grating lens-based optical delay line (GLD)[27] to implement 2-D OCT imaging in real time. By properly choosing the components of the optical delay unit (e.g., focal length $f = 80$ mm for the achromatic lens, groove density $D = 450$ lines/mm for the diffraction grating, and tilting angle $\theta = 7.5$ deg for the servomirror) an optical delay window or depth scan of 2.8 mm or higher at the rate of up to 2.4 kHz was obtained (both forward and backward cycles were used), which is sufficient for the speed requirements of most *in vivo* 2-D OCT imaging.

By carefully adjusting the positioning of the dispersion grating off the front focal plane of the Fourier lens, the excessive group dispersion can be reduced, yielding a measured coherence length $L_c = 10\ \mu$m that is very close to the source coherence length. Light from both the sample and the reference arms was combined at the output fiber; detected by a PIN detector; followed by a low-noise preamplifier, a bandpass filter, and an envelope detector for analog signal processing; and was then digitized by a 5-MHz, 12-bit analog to digital (A/D) converter. A Pentium IV computer displayed and stored the 2-D OCT image sequences acquired and displayed at roughly five frames/s during the arthroscopic examination.

Figure 2 is a schematic showing the optical layout within the probe and a photograph of the hand-held arthroscopic OCT probe, which includes a fiber optic collimator attached to a polarizing beam splitter (PBS), a servomirror, a laser scan lens, and an elliptical thin brass tube (autoclavable) with an angled optical window at its distal end face. Light emitted from the sample arm of the fiber optic Michelson interferometer was collimated to a ϕ2.8 mm Gaussian beam by a snap-on rotary polarizing fiber optic aspherical lens (CM), deflected laterally (θ) by a 3.5-mm servomirror (S), and focused by an achromatic lens (f) onto the cartilage surface under examination. Because the optical scan angle (θ_0) is double that of the mechanical scan angle of the servomirror, i.e., $\theta_0 = 2\theta$, the transverse scan range of the arthroscopic OCT probe, L, is given by

$$L = 2f \times tg(2\theta) \approx 4f\theta. \tag{1}$$

Large angular scans at up to ± 15 deg could be provided, but the lateral scanning range, L, was eventually limited by the transverse size allowance of the arthroscopic OCT probe. For the elliptical scope sheath used in this study, the diameters of the long and short axes of the oval cross-section were 7.5 and 3 mm, respectively, and the effective lateral scanning range for 2-D arthroscopic OCT imaging was $L \approx 6$ mm, which is sufficient for *in vivo* cartilage imaging. A simple rotary PBS was used to discriminate cartilage structural lesions from polarization- or birefringence-induced artifacts, as will be discussed later.

For the hand-held OCT probes used in this study, the distal end face was sealed or terminated by an angled glass window rather than by the scan lens, as was done in the previous designs. The advantages of this improved probe design are as follows. First, it almost doubled the depth of the arthroscope that could be inserted into the joint tissue. The focal length of the scan lens, f, was either 40 or 60 mm, and the probing tube of the scope that could be inserted into joint tissue, d

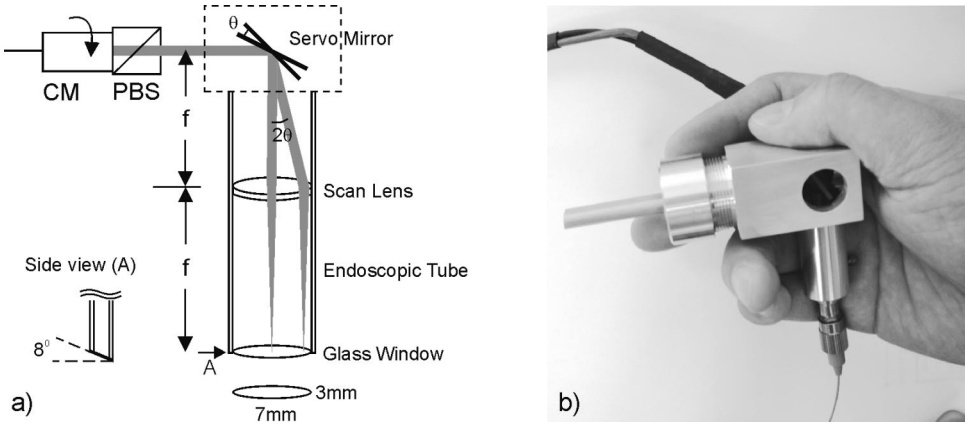

Fig. 2 Arthroscopic OCT probe. (a) A schematic diagram of the OCT probe. (b) A photograph of the hand-held OCT arthroscopic probe. PBS, polarization beam splitter attached to the rotary fiber optic collimator.

($\approx 2f$), was either 70 or 110 mm, which is deep enough for most uses to examine human knee joint cartilage. Second, because the distal end face of the elliptical tube was sealed with a 100-μm-thick optical-grade glass slide angled at 8 deg, it protected the optical components (e.g., scan lens) within the tube from fluid contamination during *in vivo* examination and minimized the specular back-reflection, which drastically reduced the coherence noise induced by side lobes of the BBS source and thus maintained a high signal-to-noise (SNR) ratio. Third, the OCT arthroscopy was able to achieve ''focus-free'' examination. This was because the length of the elliptical tube was precisely engineered to ensure that when the OCT probe was immersed in saline or body fluid, the focal plane was projected on the perpendicular cross-section at the further edge of the angled window-as indicated in Fig. 2. This optical arrangement permitted the cartilage sample under examination to be in focus as soon as the distal edge of the OCT probe was in contact with the cartilage surface, which proved to be effective for instantaneous optical alignment and reduction of artifacts induced by the movement of living tissue during *in vivo* endoscopic procedures. Most important, this optical layout prevented the substantial degradation of OCT image contrast and resolution caused by absorption of body fluid and the degraded spherical aberration. (Most commercial lenses, including the scan lens used, are designed for optimizing spherical aberration in free space with a refractive index of $n=1$ rather than in body fluid with $n>1.33$.)

In order to study the influence of absorption of body fluid (primarily by water[28]) at 1.3 μm on OCT contrast, which has been neglected so far, we performed simulation experiments on changes in OCT contrast of a mirror and a piglet cartilage specimen immersed at different depths in saline. In the experiments, the specimens placed on a motored 3-D stage were carefully adjusted to ensure that the surface of the samples (e.g., mirror) were in focus. The results (Fig. 3) indicated a substantial absorption loss of light and degradation in OCT image contrast in saline. Based on the results, we extended the sheath to enclose the path from the scan lens to the focal plane, which was found to immensely enhance the OCT image contrast and resolution compared with the previous designs with the distal end face terminated by the scan lens.

Both depth scan in the reference arm and lateral servoscan in the arthroscope were synchronized with the image data acquisition via two 16-bit D/A channels. The axial resolution Δz and the lateral resolutions ΔL of the OCT arthroscope are defined by the source coherence length and the scan lens,[15]

$$\Delta z = L_C = (4\sqrt{\ln 2}/\pi) \times (\overline{\lambda^2}/\Delta\lambda) \tag{2}$$

$$\Delta L = 2\overline{\lambda}/\pi NA = 4\overline{\lambda} f/\pi\phi, \tag{3}$$

where $NA=\phi/2f$ is the numerical aperture of the scan lens. For the arthroscopic OCT setup used in this study, they were roughly 10 and 17 μm, respectively.

3 Test Results

To demonstrate the capability of the hand-held OCT probe for near real-time laser scanning arthroscopy, we imaged the articular cartilage in pig knee joints to test the image fidelity and feasibility for imaging mammalian knee joints. *In vivo* OCT arthroscopy was performed on the hindlimb knee joints of Hanford minipigs weighing roughly 42 kg each. Using standard arthroscopic techniques, two ϕ8-mm holes were created through skin and capsule using an 11-0 surgical blade. An anterolateral portal was used for arthroscopic guidance and a transpatellar tendon portal was used for OCT imaging and biopsy. Figure 4(a) illustrates the arthroscopic procedure and Fig. 4(b) is a digitized video frame taken by a 3 CCD camera in the 30-deg arthroscope to locate the geometric positions of the OCT probe and the cartilage to be imaged. The 30-deg arthroscope was inserted in the knee joint first and moved to the surface area of the articular cartilage of interest. Next, the OCT probe was inserted and video guided by the arthroscope until it reached the preselected imaging spot. Precise alignment of the OCT probe both axially and laterally was guided by near real-time 2-D OCT images (i.e., five frames/s movies) displayed on a PC monitor. Because of our unique focus-free probe design, the arthroscopic OCT imaging procedure was easy to handle.

Arthroscopic imaging of normal porcine knee cartilage using the hand-held probe produced OCT images comparable in size, resolution, and contrast to those of *ex vivo* OCT.[25] Figure 5 shows the results of normal porcine cartilage before and

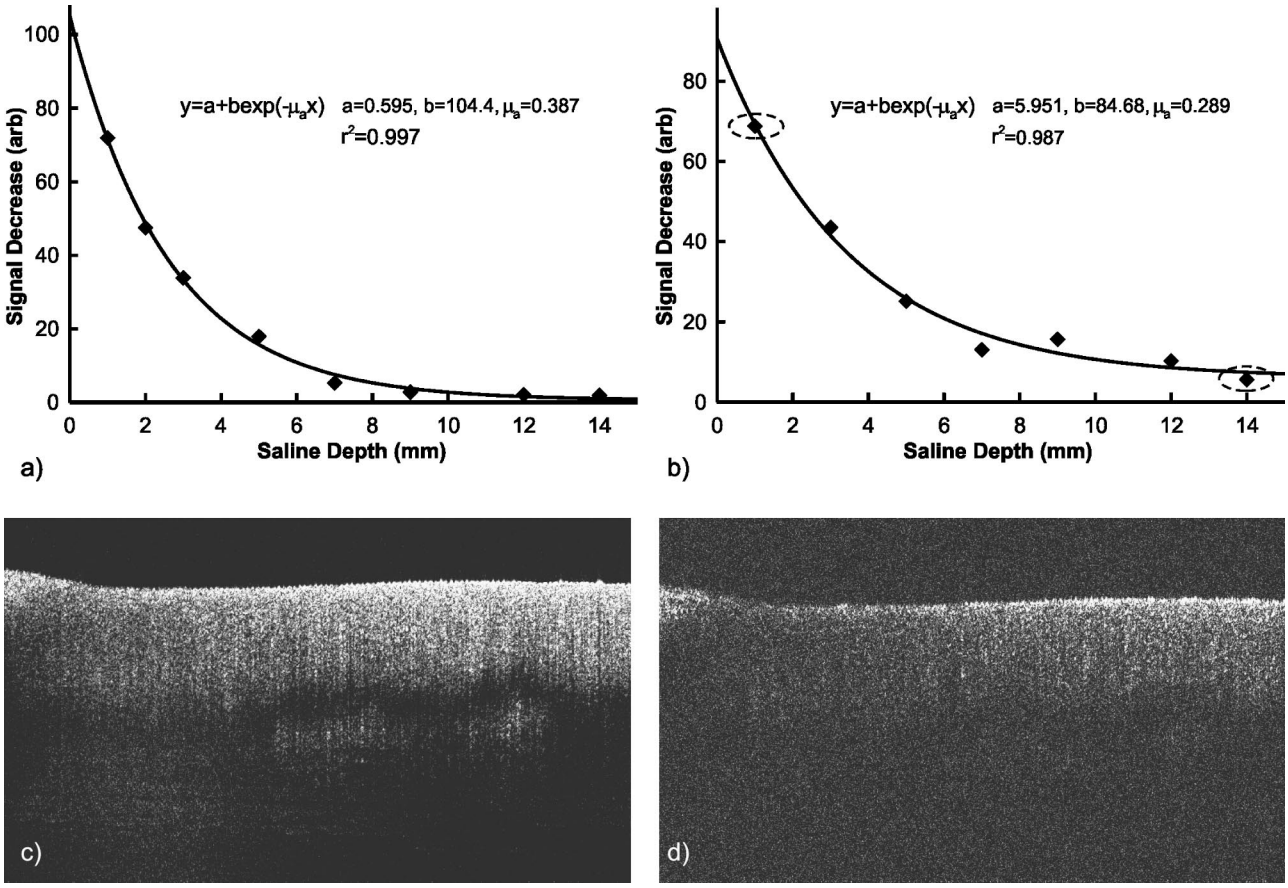

Fig. 3 OCT signal change as a function of the depth of fluid immersion. (a) OCT signal change versus the depth of a mirror immersed in saline. (b) OCT signal change versus the depth of a porcine cartilage immersed in saline. (c) 2-D OCT image of cartilage immersed 1 mm below saline. (d) 2-D OCT image of cartilage immersed 14 mm below saline. The dotted points in (a) and (b) were measured results; the solid lines are results acquired by a least-squared fit. Typical signal-to-noise ratios in (c) and (d) decreased from 52 to 27 dB. OCT image size: 6 mm lateral and 2 mm vertical. The dashed circles in (b) indicate the depths at which (c) and (d) were imaged.

after surgical treatment. Figure 5(a) is an *en face* RGB image of the cartilage surface taken by a conventional 30-deg arthroscope whereas Fig. 5(b) is a 2-D arthroscopic cross-sectional OCT image of the articular cartilage shown in Fig. 5(a). The OCT image is displayed in pseudocolor and a color bar is illustrated in which the bright-to-dark transition indicates the high-to-low backscattering scale in the OCT image. The image size is 6 mm wide and 2 mm deep, assuming that the refractive index of cartilage tissue is approximately 1.50. The normal cartilage tissue appeared as a relatively uniform band in the OCT image except for a horizontal shadow, as indicated by the arrows. This subsurface horizontal shadow is induced by cartilage birefringence and is further discussed in relation to Fig. 8.

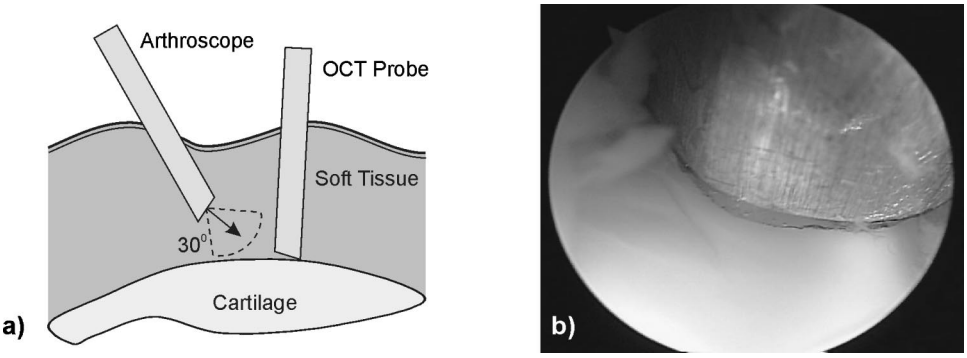

Fig. 4 Arthroscopic OCT imaging of cartilage tissue *in vivo*. (a) A sketch to illustrate the OCT arthroscopy procedure. (b) A digitized color image taken by the 3CCD camera in the arthroscope. A conventional 30-deg arthroscope was used to move the OCT arthroscope to select the spot of interest on the cartilage to be imaged.

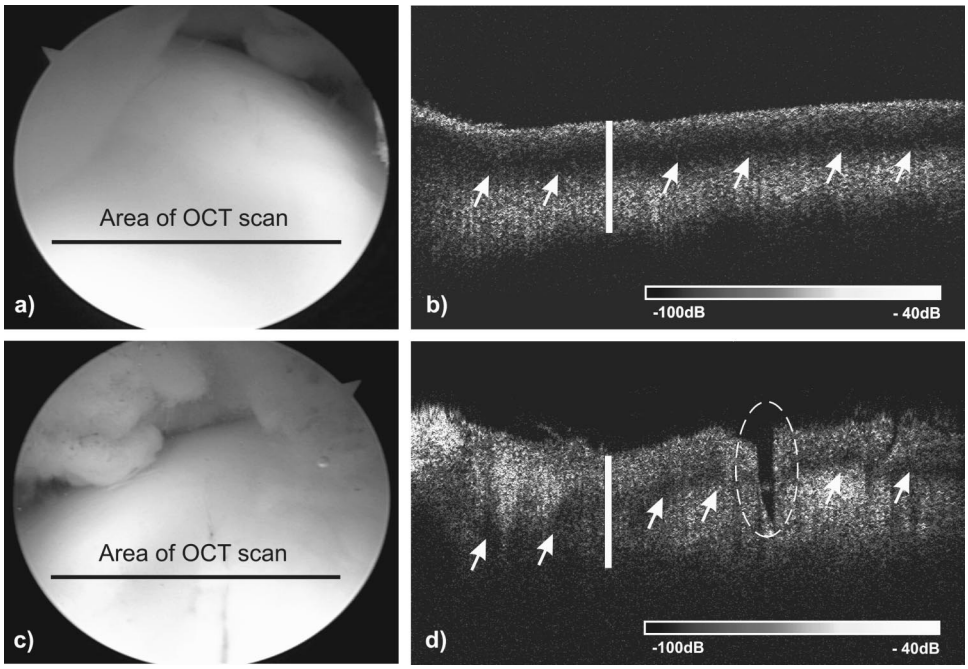

Fig. 5 *In vivo* arthroscopic imaging of normal procine cartilage before and after a surgical incision. (a) *En face* RGB image of the cartilage surface taken by a conventional 30-deg arthroscope. (b) 2-D cross-sectional OCT image underneath the cartilage surface shown in (a). (c) *En face* RGB image of the cartilage surface postincision. (d) 2-D cross-sectional OCT image underneath the cartilage surface shown in (c). The image size for (a) and (c) is roughly ϕ 10 mm, and the image size for (b) and (d) is roughly 6 mm wide and 2 mm deep. The arrows in (b) and (d) indicate the interfaces of cartilage layers with different collagen fiber orientations, causing form birefringence in the OCT image. The dark lines in (a) and (c) indicate the area to be scanned by OCT probe. The white bars in (b) and (d) indicate the full thickness of the porcine cartilage. The dashed circle in (d) shows a 0.24-mm-wide, 0.67-mm-deep incision.

Because the porcine cartilage was thinner than 2 mm, the full cartilage thickness could be measured. By OCT assessment, the cartilage was between 0.76 and 0.84 mm thick. To test the utility of OCT arthroscopy in instantaneous, *in vivo* diagnosis of subsurface cartilage injury or defects (e.g., fibrillations), the same normal cartilage was incised using a bone cutter. Figure 5(c) shows the incision on the cartilage surface, whereas Fig. 5(d) shows the cross-sectional OCT image of the treated area. While the incision was visible with conventional *en face* arthroscopic imaging, OCT allowed both visualization and measurement of the cross-section of the small 0.24-mm wide, 0.67-mm deep injury.

To further demonstrate the utility of OCT arthroscopy for instantaneous assessment of therapeutic effects, we performed experiments to examine the sensitivity of the OCT arthroscope in evaluating radiofrequency (RF) treatment of porcine cartilage. Figure 6 shows that even at a very low RF energy level (Arthrocare ACD-50: 200 V, 1.25 mm/s), the OCT image in Fig. 6(a) was able to detect the backscattering decrease (i.e., the shadow in the dashed circle) as a result of RF coagulation. By comparison with the corresponding histology in Fig. 6(b), these two imaging modalities can provide important information for immediate diagnosis and assessment of morphological changes below the cartilage surface following RF treatment. While fluorescence imaging [Fig. 6(b)] requires removal of tissue, OCT imaging provides comparable diagnosis instantaneously during arthroscopy.

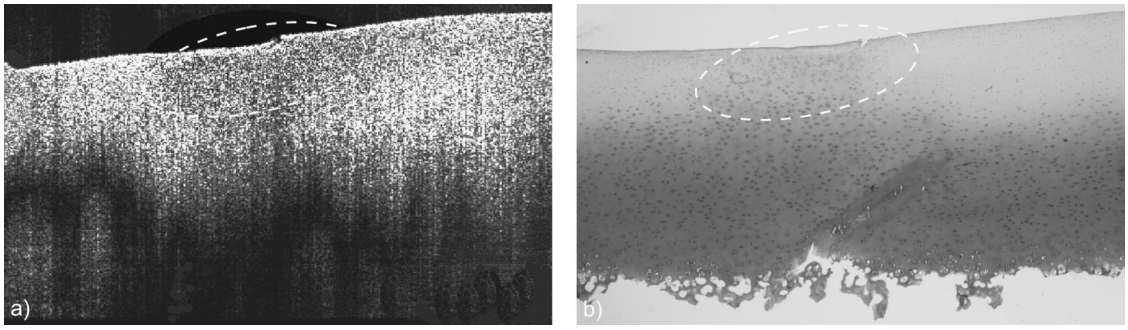

Fig. 6 *In vivo* arthroscopic OCT of porcine cartilage following RF coagulation. (a) 2-D OCT showed a backscattering decrease indicative of structural changes in the treated cartilage subsurface. (b) Safranin O-stained histology with fast green counterstaining (red staining is for proteglycan). Image size: roughly 6 mm wide and 2 mm deep. The white dashed circles indicate the area under RF coagulation.

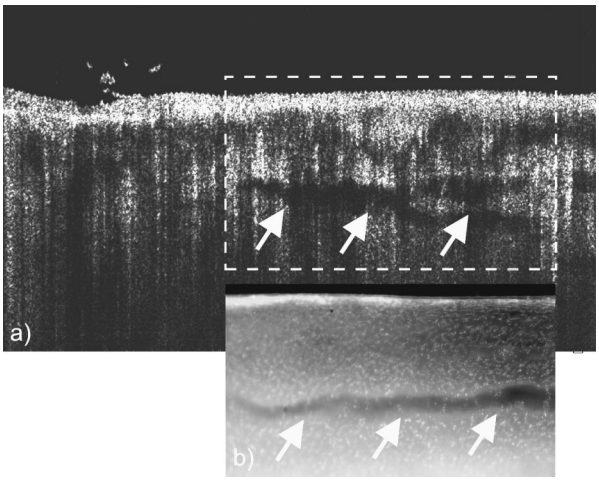

Fig. 7 *Ex vivo* arthroscopic OCT of an embedded cartilage tear (a) 2-D OCT clearly delineated a minute cartilage tear that was less than 0.2 mm thick but embedded 0.6 mm below the cartilage surface. (b) Green fluorescent dye-stained histology from a parallel cross-section of the dashed area in (a). Image size: roughly 6 mm wide and 2 mm deep for (a); 3.6 mm wide and 1 mm deep for (b). The white arrows in both images indicate the embedded tears.

In addition to cartilage surface smoothness, detection of embedded subsurface minute tears is critical to the early diagnosis and prevention of osteoarthritis. Figure 7 demonstrates the unique potential of OCT arthroscopy for the high-resolution imaging of cartilage injury. Figure 7(a) is the OCT image in which a subsurface cartilage tear that was invisible to regular arthroscopy was clearly delineated and correlated well with the histological result of the parallel cross-section, as indicated by arrows.

As indicated by the arrows in Fig. 5, even normal cartilage tissue might show ''ghost'' shadows (banding effect) in OCT images. According to previous *ex vivo* studies of ours and of others,[19–23] these subsurface ''ghost'' shadows may be caused by form birefringence induced by differing orientation of collagen fibrils within the articular cartilage (most likely in zones 2 to 4 in cartilage, where the orientation of fibrils gradually changes to become parallel to the cartilage surface); therefore, if partially polarized or linearly polarized light was illuminated, because of the additional phase shift induced by the form birefringence of the oriented fibrils, the two orthogonally polarized light beams backscattered from the tissue might constructively and destructively interfere, and as a result produce the ''ghost'' patterns (e.g., destructive interference). This effect can be examined by a simple comparison with the polarized OCT and is shown in Fig. 8, in which Fig. 8(b) shows the diminished banding effect by rotating the polarizer. The ''ghost'' patterns might be artifacts in OCT images misidentified as tissue boundaries. However, they can be easily differentiated by polarizing OCT [Fig. 8(b)] in which the ghost patterns were minimized by rotating the polarization plane in the probe (i.e., CM with attached PBS). More important, because they resulted from differing collagen fibril orientations, the ''ghost'' patterns might provide morphological characteristics of the structural integrity of cartilage tissue.[22] Our recent *ex vivo* human studies suggested that loss of polarization contrast (e.g., ''ghost'' patterns) in OCT imaging was related to cartilage degeneration and injury, which may provide useful diagnosis of early osteoarthritic cartilage. However, a distinctive detection of detailed cartilage birefringence distribution requires a true polarization-sensitive OCT that simultaneously detects two orthogonal polarization OCT signals or even the Muller matrix of cartilage.[23] We are in the process of incorporating our hand-held probe design with other reported PSOCT techniques.[22–24]

4 Discussion

Previous *ex vivo* studies based on human and animal cartilage models demonstrated that OCT was able to delineate cartilage structure and micromorphology to show pathological changes such as fibrillation, subsurface tears, tissue damage, and degeneration, thus justifying the development of OCT arthroscopes for clinical diagnosis of cartilage injury and immediate assessment of therapeutic treatments.[25] In this paper we present a novel hand-held polarization OCT arthroscope and preliminary results based on an *in vivo* porcine study to examine the practicality and the utility of the OCT arthroscope for future use on humans. The optical design of the OCT probe enables the transverse and axial resolutions of the imaging system to be roughly 17 and 10 μm, respectively. Two-dimensional cross-sectional images of cartilage tissue with 500×1000 pixels covering an area 6 mm wide and 2 mm deep can be acquired at nearly five frames/s and with over 100 dB of dynamic range. Furthermore, the unique optical configuration in the OCT scope can substantially reduce the specular

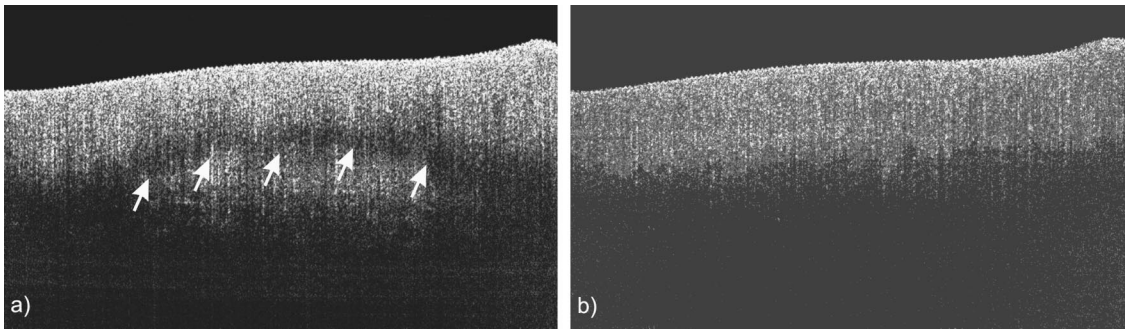

Fig. 8 *In vivo* arthroscopic OCT images of a normal porcine cartilage with the polarization angle changed. Image size: roughly 6 mm wide and 2 mm deep. The arrows in (a) indicate the "ghost patterns" that represent the interfaces of cartilage layers with different collagen fiber orientations, which resulted in form birefringence in the OCT image. (b) By rotating the polarization plane (possibly close to or vertical to the fast axis of the collagens in the cartilage) the banding effect was reduced.

back-reflection of the probe end face (Fig. 2) and body fluid absorption at 1.3 μm (Fig. 3), and ensures that the OCT scanner is in focus as long as the probe touches the cartilage specimen to be examined. The test results shown in Fig. 4 demonstrate that the OCT probe can be easily used with a conventional 30-deg arthroscope for cartilage site guidance and can acquire high-resolution OCT images of cartilage in near real time. Not only can it provide cross-sectional morphologies of normal porcine articular cartilage (Fig. 5), but it can also detect and measure an injury made with a surgical instrument (Fig. 5), backscattering changes induced by RF treatment (Fig. 6), and embedded minute cartilage tears (Fig. 7), suggesting its potential for immediate imaging assessment of minimally invasive therapeutic treatments of cartilage injury. Although the rotary polarizing OCT probe may be unable to provide detailed cartilage birefringence distribution, our preliminary results (e.g., Fig. 6 to Fig. 8) show that this simple, inexpensive attachment can discriminate structural defects from birefringence-induced artifacts (''ghost patterns'').

Minimally invasive arthroscopic removal and stabilization of fibrillated cartilage surfaces using surgical incision—mechanical shaver and radiofrequency ablation—has been widely used for clinical treatment of osteoarthritic cartilage. The assessment of different therapeutic protocols has been hampered by the inability to obtain cross-sectional information without resorting to destructive histology. The obvious advantages of arthroscopic OCT for these applications are that OCT assessment is instantaneous, noninvasive, and nondestructive, below the surface, and at high resolution. In summary, we have successfully developed a novel hand-held OCT arthroscope for *in vivo* and high-resolution imaging of cartilage morphology and injuries. Successful application to porcine cartilage imaging *in vivo* demonstrates the resolution and practicality of the OCT arthroscope for use in human examinations.

Acknowledgments

This work is supported in part by National Institutes of Health contracts R01-DK059265 (YP) and R21-AR046995 (CC), the Whitaker Foundation contract 00-0149 (YP), and the Pittsburgh Tissue Engineering Initiative (YP).

References

1. B. Chance, K. Kang, and E. Sevick, ''Photon diffusion in breast and brain: spectroscopy and imaging,'' *Opt. Photonics News* **4**, 9–13 (1993).
2. M. Rajadhyaksha, M. Grossman., D. Esterowitz, R. Webb, and R. R. Anderson, ''*In vivo* confocal scanning laser microscopy of human skin: melanin provides strong contrast,'' *J. Invest. Dermatol.* **104**, 946–952 (1995).
3. W. Denk, J. W. Piston, and W. W. Webb, ''Two-photon molecular excitation in laser scanning microscopy,'' *Science* **248**, 73–76 (1990).
4. J. G. Fujimoto, ''Optical coherence tomography: a new view toward biomedical imaging,'' *Photonics Spectra* **32**(1), 114–115 (1998).
5. D. Huang, E. A. Swanson, C. P. Lin, J. S. Schuman, W. G. Stinson, W. Chang, M. R. Hee, T. Flotte, K. Gregory, C. A. Puliafito, and J. G. Fujimoto, ''Optical coherence tomography,'' *Science* **254**, 1178–1181 (1991).
6. J. S. Schuma, C. Puliafito, and J. G. Fujimoto, *Optical Coherence Tomography of Ocular Diseases*, 2nd ed., Slack, Thorofare, NH (1993).
7. Y.-T. Pan and D. L. Farkas, ''Dual-color, 3-D imaging of biological tissues using optical coherence tomography,'' *J. Biomed. Opt.* **3**(4), 446–455 (1998).
8. B. W. Colston, Jr., U. S. Sathyam, L. B. DaSilva, M. J. Everett, P. Stroeve, and L. L. Otis, ''Dental OCT,'' *Opt. Express* **3**(6), 230–238 (1998).
9. G. J. Tearney, M. E. Brezinski, B. E. Bouma, S. A. Boppart, C. Pitris, J. F. Southern, and J. G. Fujimoto, ''*In vivo* endoscopic optical biopsy with optical coherence tomography,'' *Science* **276**, 2037–2039 (1997).
10. K. Kobayashi, J. A. Izatt, M. D. Kulkarni, J. Willis, and M. V. Sivak, Jr., ''High-resolution cross-sectional imaging of the gastrointestinal tract using optical coherence tomography: preliminary results,'' *Gastrointest Endosc.* **47**, 515–523 (1998).
11. Y. Pan, J. P. Lavelle, S. I. Bastacky, S. Meyers, G. Pirtskhalaishvili, M. L. Zeidel, and D. L. Farkas, ''Detection of tumorigenesis in rat bladders with optical coherence tomography,'' *Med. Phys.* **28**(12), 2432–2440 (2001).
12. B. Bouma, G. Tearney, S. Boppart, M. R. Hee, M. Brezinski, and J. G. Fujimoto, ''High-resolution optical coherence tomographic imaging using a mode-locked Ti:Al_2O_3 laser source,'' *Opt. Lett.* **20**, 1486–1488 (1995).
13. J. F. de Boer, S. Srinivas, A. Malekafzali, Z. P. Chen, and J. S. Nelson, ''Imaging thermally damaged tissue by polarization-sensitive optical coherence tomography,'' *Opt. Express* **3**(6), 212–129 (1998).
14. Z. Chen, T. E. Milner, D. Dave, and J. S. Nelson, ''Optical Doppler tomographic image of fluid flow velocity in highly scattering media,'' *Opt. Lett.* **22**, 64–66 (1997).
15. U. Morgner, W. Drexler, F. X. Kärtner, X. D. Li, C. Pitris, E. P. Ippen, and J. G. Fujimoto, ''Spectroscopic optical coherence tomography,'' *Opt. Lett.* **22**, 111–113 (2000).
16. F. I. Feldchtein, G. V. Gelikonov, V. M. Gelikonov, R. V. Kuranov, A. M. Sergeev, N. D. Gladkova, A. V. Shakhov, N. M. Shakhova, L. B. Snopova, A. B. Terent'eva, E. V. Zagainova, Y. P. Chumakov, and I. A. Kuznetzova, ''Endoscopic applications of optical coherence tomography,'' *Opt. Express* **3**(6), 257–270 (1998).
17. Y. Pan, H. Xie, and G. Fedder, ''Endoscopic optical coherence tomography based on a microelectromechanical mirror,'' *Opt. Lett.* **26**(24), 1966–1968 (2001).
18. C. Cooper, S. Snow, and T. McAlindon, ''Risk factors for the incidence and progression of radiographic knee osteoarthritis,'' *Arthritis Rheum.* **43**, 995–1000 (2000).
19. J. Herrmann, C. Pitris, B. E. Bouma, S. A. Boppart, J. G. Fujimoto, and M. E. Brezinski, ''High resolution imaging of normal and osteoarthritic cartilage with optical coherence tomography,'' *J. Rheumatol.* **26**, 627–635 (1999).
20. I. Y. Jong, G. Vargas, M. G. Ducros, S. A. Telenkov, B. J. Wong, and T. E. Milner, ''Thermally induced birefringence changes in cartilage using polarization-sensitive optical coherence tomography,'' *Proc. SPIE* **4257**, 213–220 (2001).
21. K. A. Hansen, J. K. Barton, and J. A. Weiss, ''Optical coherence tomography imaging of collagenous tissue microstructure,'' *Proc. SPIE* **3914**, 581–587 (2000).
22. W. Drexler, D. Stamper, C. Jesser, X. Li, C. Pitris, K. Saunders, S. Martin, M. B. Lodge, J. G. Fujimoto, and M. E. Brezinski, ''Correlation of collagen organization with polarization sensitive imaging of *in vitro* cartilage: implications for osteoarthritis,'' *J. Rheumatol.* **28**(6), 1311–1318 (2001).
23. S. Jiao and L. H. Wang, ''Jones-matrix imaging of biological tissues with quadruple-channel optical coherence tomography,'' *J. Biomed. Opt.* **7**(3), 350–358 (2002).
24. C. E. Saxer, J. F. de Boer, B. H. Park, Y. Zhao, Z. Chen, and J. S. Nelson, ''High-speed fiber-based polarization-sensitive optical coherence tomography of *in vivo* human skin,'' *Opt. Lett.* **25**(18), 1355–1357 (2000).
25. C. W. Han, C. R. Chu, N. Adachi, A. Usas, F. H. Fu, J. Huard, and Y. T. Pan, ''Analysis of rabbit articular cartilage repair after chondrocyte implantation using optical coherence tomography,'' *Osteoarthritis Cartilage* (submitted).
26. J. F. de Boer and T. E. Milner, ''Review of polarization-sensitive optical coherence tomography and stokes vector determination,'' *J. Biomed. Opt.* **7**(3), 359–371 (2002).
27. G. J. Tearney, B. E. Bouma, and J. G. Fujimoto, ''High-speed phase and group-delay scanning with a grating-based phase control delay line,'' *Opt. Lett.* **22**(23), 1811–1813 (1997).
28. L. Kuo, D. Labrie, and P. Chylek, ''Refractive indices of water and ice in the 0.65–2.5 μm spectral range,'' *Appl. Opt.* **32**, 3531–3540 (1993).